Effect of Aluminium on Mechanical Properties of low strength low alloy Welds

[1]Rakesh Sharma, [2]Vishnu Singh, [3]Manvendra Singh
[1]Assistant Professor, [2]Assistant Professor, [3]Assistant Professor
IIMT Group Of Colleges

Abstract **- The effect of filler metal composition on the microstructure and mechanical prop erties of fourwire tandem submerged arc welded API 5LX65 steel was investigated. Microhardness, izod impact, and allweld longitudinal round tensile tests were ap plied to evaluate the mechanical properties of the weld metals. The microstructure of specimens was studied by optical and scanning electron microscopes. The structural observations showed that the more acicular ferrite was formed in the microstructure, the better mechanical properties were achieved. The impact energy and strength values were higher for the specimen containing more amounts of tita nium and boron. The brittletoductile transition temperature could be decreased by increasing the amount of acicular ferrite. For the microstructure with 80% acicular ferrite, the impact energy was about 70 J at –60°C. The addition of titanium dispersed fine oxide inclusions and facilitated the nucleation of acicular ferrite in the microstructure. The oxide particles with a size of 2 µm acted as the nucleation sites of acicular ferrite.**

keywords **- Mechanical Properties, Filler Metal, Tandem Submerged Arc Welding (TSAW), Microstructure, API 5LX65 Pipe**

INTRODUCTION

High-strength low-alloy (HSLA) steels, which have a good combination of strength and toughness, have been widely used in the construction of long-distance oil and gas pipelines (Refs. 1–7). Although formability, fracture toughness, resistance to hydro-gen-induced cracking (HIC), stress corrosion cracking (SCC) behavior, sulfide stress cracking (SSC) resistance, and fatigue strength are the workability requirements, weldability is one of the most important necessities for pipeline steels (Refs. 7–11).

The mechanical properties of welds are influenced by chemical composition, cooling rate (related to heat in- put), and microstructure. Microstructure is particularly a function of the other variables. Chemical composition is the most important factor deter- mining the weld metal (WM) proper- ties (Ref. 12). The electrode composition, type of flux, base metal dilution, and pyrometallurgical chemical reactions in the weld arc could affect the weld metal composition (Refs. 9, 12, 13). In order to improve the WM toughness, two major accesses, including the use of different fluxes (Ref. 9) and the change of filler metals, have been followed (Refs. 7, 8).

It has been shown that a predominant acicular ferrite (AF) microstructure with martensite/austenite (M/A) is- lands as a second phase showed the highest resistance to cleavage fracture due to the existence of fine interlocking laths of AF phase (Refs. 14–16). Conversely, cracks could propagate easily through the microstructure containing blocky proeutectoid ferrite (Ref. 14).

It is well known that the alloying elements such as Ni, Mo, Cr, Nb, and Ti have a considerable effect on the microstructure (Refs. 7, 13, 17). According to Bhole et al. (Ref. 7), the combined presence of Ni (2.03–2.91 wt-%) and Mo (0.7–0.995 wt-%) resulted in an increase in AF. On the other hand, when Ni was added alone in the range of 2.03–3.75 wt-%, the weld metal showed a lower toughness value due to the reduced amount of AF and the in- creased volume fraction of ferrite with second phase (FS). In the case of silicon, acicular ferrite could be formed in the microstructure when the Si con- tent was relatively low, i.e., 0.03–0.26 wt-% (Ref. 6). At higher Si contents between 0.42 and 0.95 wt-%, AF was not observed and the microstructure was close to bainite.

It has been reported that boron segregates to the grain boundaries and reduces the boundary energy; as a result, heterogeneous nucleation is prohibited and the amount of allotriomorphic ferrite and bainite is reduced. This phenomenon

Fig. 1-A-The schematic view of the welding pass sequence; B-TSAW configuration of electrodes; C-welding on the inside

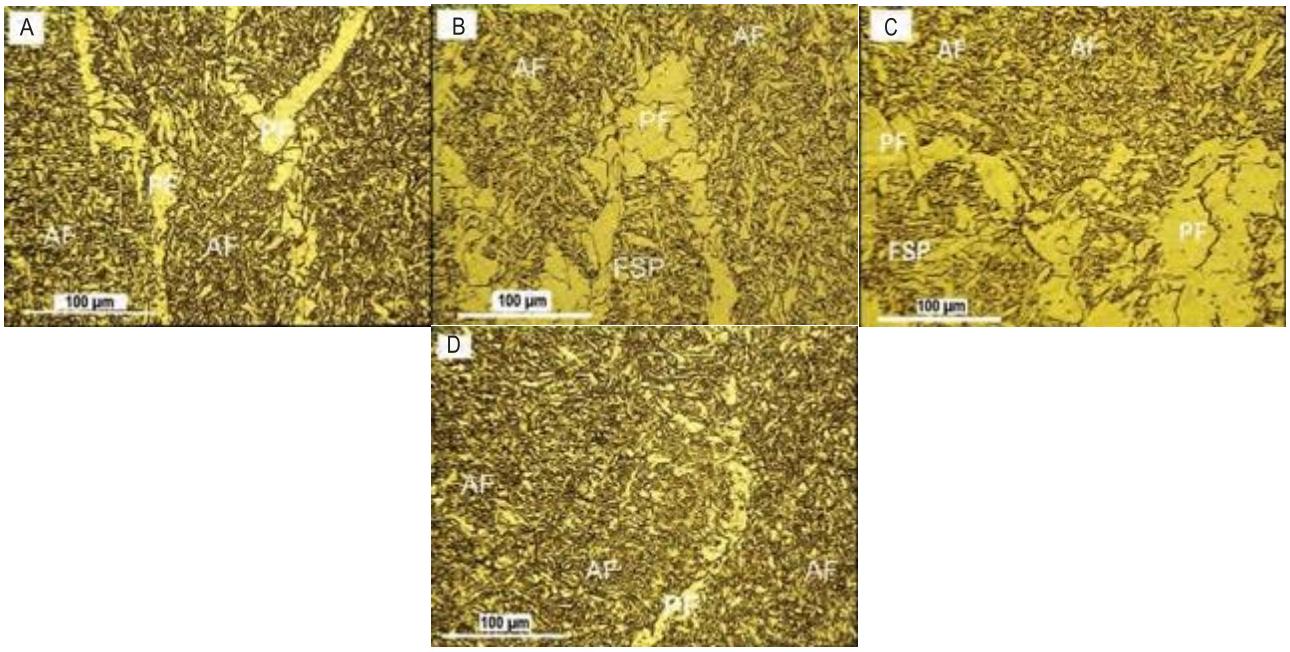

Fig. 2- Optical micrographs of OD region. A-Specimen , B-Specimen B, C-specimen C, D-Specimen D

allows AF to form at inclusions, and the hardenability is promoted (Refs. 18–20). Boron has a high tendency to form compounds with O_2 and N_2; therefore, titanium is usually added to the weld wire to protect the boron. Furthermore, titanium makes boron more available for the grain boundary segregation by entrapping C and N (Ref. 20). This fact is the reason for the development of the Mo-Ti-B wires in the sub- merged arc welding (SAW) process (Ref. 14). Also, titanium improves the tough- ness of steel weldments and refines the microstructure by forming stable Ti-rich particles (Refs. 21, 22). Increasing Ti content of the weld metal leads to an in- crease in the number of inclusions, which act as nuclei for acicular ferrite formation (Ref. 6).

Table 1 — Effect of Alloying Elements on Phase Distribution and Mechanical Properties of Steel Weldments

Alloying Elements (wt-%)				Phase Distribution			Mechanical Properties (+ or –)	Material (WM)	
Ni	Mo	Mn	Si	AF	GBF	FS			
–	0.81–0.88	–	–	Increase	Increase	–	Positive		
2.03–2.91	0.7–0.99	–	–	Increase	Decrease	Decrease	Positive		
2.03–3.75	–	–	–	Decrease	–	Increase	Negative	HSLA-X70	Ref. 7
More than 1.02	–	1.55-1.59	–	Decrease	–	Increase	Negative		
–	0.25	1.50	–	Increase	–	–	Positive	C- Steel	Ref. 23
More than 2.25	–	1.40	–	Decrease	–	–	Negative	C-Mn Steel	Ref. 24
–	Up to 0.20	–	–	Increase	Decrease	–	Tensile Strength (Positive) Impact Toughness (Decrease)	HSLA-X80	Ref. 25
0.84	0.42	–	–	Increase	–	–	Positive	HSLA	Ref. 26
–	–	–	0.03-0.26	Increase	–	–	Positive	C-Mn Steel	Ref. 27
–	–	–	0.42–0.95		Bainitic Microstructure		Negative		

Lee et al. (Ref. 21) investigated the increase in sulfur content from 0.0005 to 0.0124% in Ti-killed steels by the simulation of the heat-affected zone (HAZ) thermal cycle. They reported that by increasing S content to 0.0102%, the amount of AF was increased, and then acicular ferrite was re placed by Widmanstätten ferrite (WF) and polygonal ferrite (PF) (Ref. 21). They explained that the dominant inclusions were changed from Ti-oxides to MnS and Ti-oxysulfides, and this could be the reason for the increased nucleation for AF. Table 1 summarizes the effect of alloying elements on the phase distribution and mechanical properties of WM.

Although extensive investigations have been done on the effect of alloying elements, this fact in the practical issues has not been studied carefully. This research investigated the effect of alloying elements in a real application of four-wire tandem submerged arc welding (TSAW).

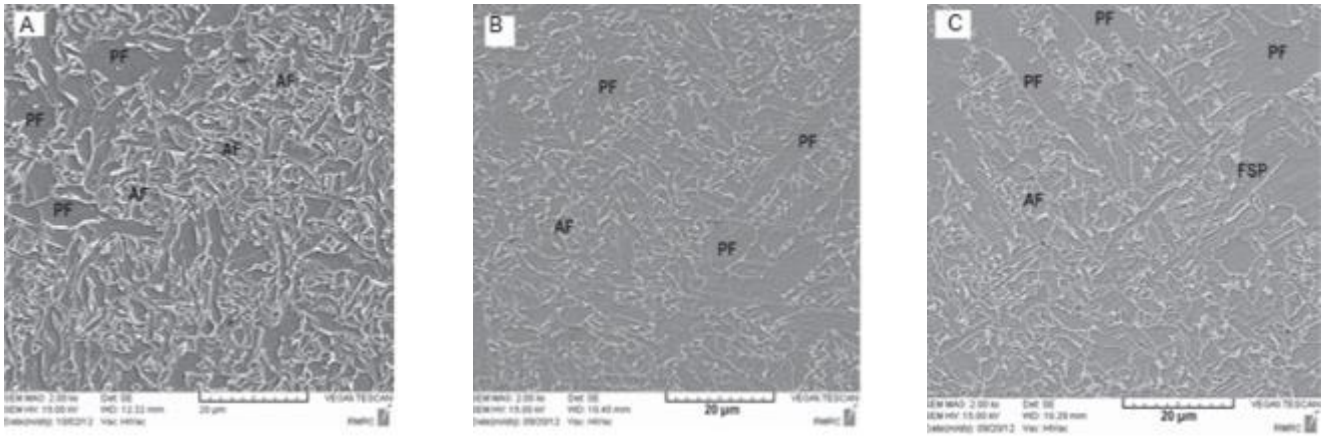

Fig. 3—SEM micrographs of the welds.

A-Specimen A B—specimen B C—specimen C

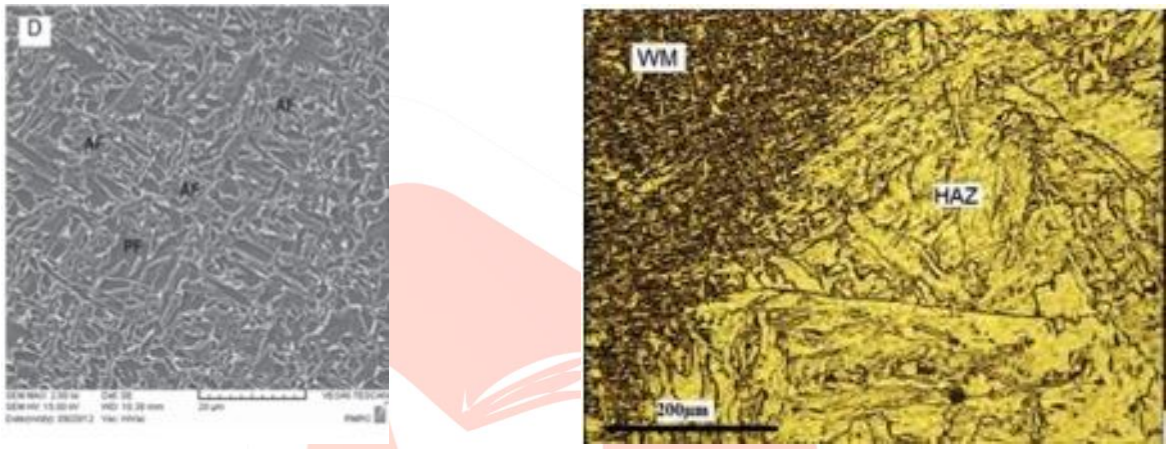

D-specimen D

Fig. 4-The microstructure of the HAZ

EXPERIMENTAL PROCEDURE

The API 5L-X65 micro alloyed HSLA steel was used as a base material with a thickness of 20.6 mm. The double-V joint preparation was used for four-wire TSAW. After being tack welded with the GMAW process, the pipe was subjected to TSAW on both sides i.e., inside and outside. Figure 1 shows the electrode configuration for the TSAW machine and the welding sequence. Four wires, with diameter of 4 mm, were used in the inner and outer passes of the TSAW process according to Table 2. The chemical composition of the wires, base met- al, and weld metals are presented in Table 3. The critical metal parameter (Pcm) was calculated based on the API- 5L specification (Ref. 28).

The Vickers micro hardness testing was done according to ASTM E-384 using a diamond pyramid indenter with a 10-kg load. The micro hardness measurements were made in a straight line parallel to the specimen surface to cover all weld regions including the HAZ and the base metal on both sides. Two standard all-weld longitudinal round tensile samples (12.5 mm diameter of the reduced section and 50-mm gauge length) were used in the tensile test according to ASTM E8. The Charpy V-notch (CVN) impact samples, which were machined in the transverse orientation (ASTM E-23: 10 × 10 × 55 mm), were tested at different temperatures, i.e.,–30, –45, –60, and –75°C.

The microstructural details were studied by optical microscopy (OM) and scanning electron microscopy (SEM). The specimens were etched with two different processes. The first group of samples was etched with Ni- tal 2% solution; while for the second group, a two-stage electrolytic method as described in Ref. 29 was used to determine the characteristics of M/A constituents and carbides. In the latter, M/A constituents are embossed and carbides are depressed in a matrix of ferrite. Therefore, M/A constituents can easily be identified by SEM. A Clemex Imagine Analysis System was used for the quantitative phase evaluation. The mode of fracture, and type of micro constituents and inclusions were determined by Tescan Vega II XMU SEM linked to a Rontec EDS system.

Table 2 — Different Combination of Wires During Welding

Specimen	Electrode No.* (Inner Passes)				Electrode No. (Outer Passes)				Flux**
	1	2	3	4	1	2	3	4	SA AB 1 67
A	S2Mo	S2Mo	S2Mo	S2Mo	S2Mo	S2Mo	S2Mo	S2Mo	AC H5
B	S2Mo	S2Mo	S2Si	S2Si	S2Mo	S2Mo	S2Si	S2Si	

C	S2Mo	S2Mo	S2Mo	S2Mo	S2Mo	S2Mo	S2Si	S2Si
D	S2Mo	S2Mo	S2Mo TB	S2Mo TB	S2Mo	S2Mo	S2Mo TB	S2Mo TB

*EN 756, **EN 760

RESULTS

The optical and SEM micrographs, as well as the volume fraction of different phases, are shown in Figs. 2 and 3, and Table 4. It can be seen from the corresponding micrographs that a mixed microstructure of polygonal ferrite (PF), acicular ferrite (AF), and ferrite with aligned second phase (FSP) was obtained in each specimen.

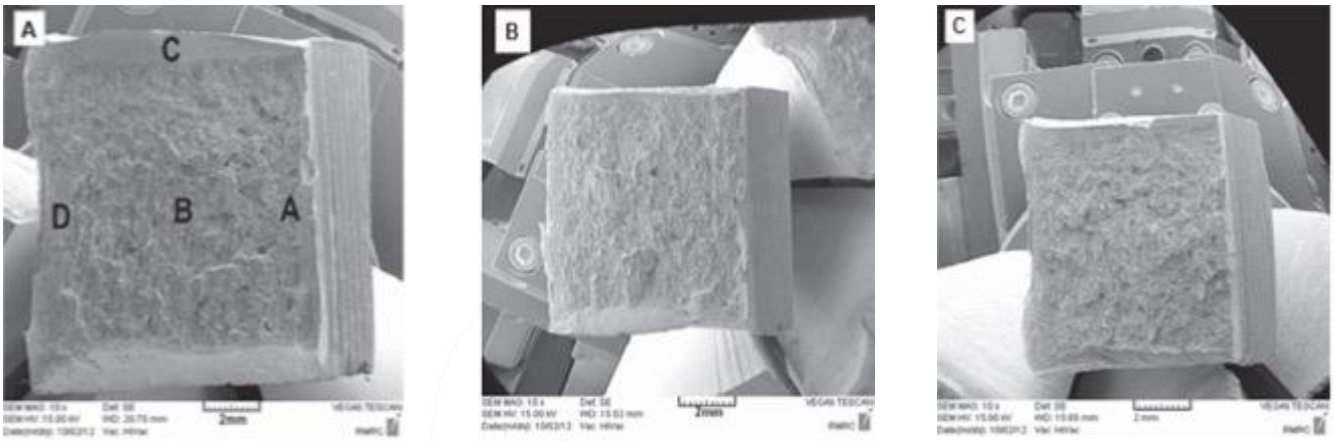

Fig.5—The macroscale fracture surface of Charpy impact test samples at–30C .

A— Specimen A B—specimen B C—specimen C

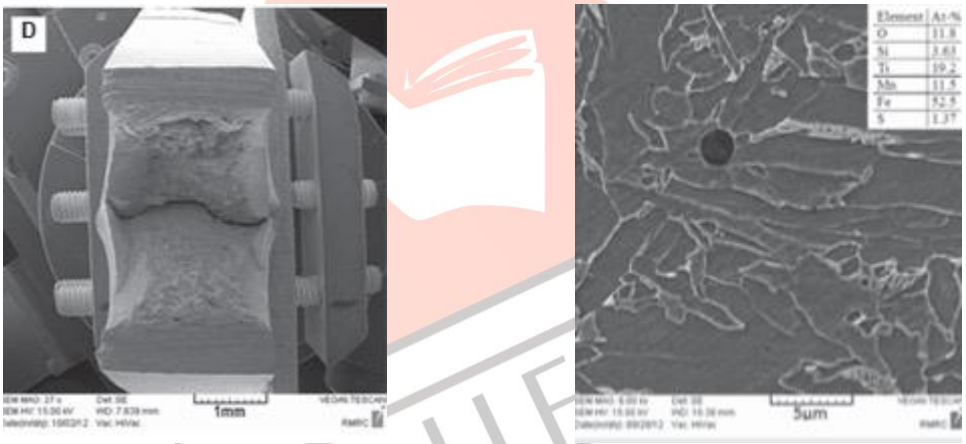

D-specimen D Fig 6. The nucleation of AF at inclusions in the weld metal

Table 4 shows the percentage of distributed phases in the weldments. It was observed that specimen D had the maximum amount of acicular ferrite (80%) and the minimum percentage of polygonal ferrite among the others. This fact could be the reason for the best mechanical properties of this specimen as will be discussed following. During the two-pass TSAW process, the HAZ produced by the first SAW pass was partly reheated by the second pass. As a result, the inter critically reheated coarse-grained HAZ (ICCG- HAZ) was produced in these joints. In this study, the ICCGHAZ of all specimens showed similar microstructural characteristics. The microstructure was a combination of ferrite and small amounts of M/A, as shown in Fig. 4. Table 5 shows the mechanical properties of WMs. The longitudinal yield strength (YS) and ultimate tensile strength (UTS) were in the range of 534–595 MPa and 606–649 MPa, respectively. Among all specimens, the highest values of yield strength, ultimate strength, and hardness were obtained in the case of weldment D. The hardness in different regions of the base metal, HAZ, inside diameter (ID), and outside diameter (OD) were in the range of 180–206, 170–208, 206–245, and 190–214 HV, respectively. The Vickers micro hardness does not vary significantly in all specimens.

Figure 5 shows the macroscale fracture surface of Charpy impact test samples at –30ºC, which consisted of four regions: the fracture initiation region close to the notch (marked as A), the main fracture region in the center of the sample (B), the shear lip regions toward the center (C), and the final fracture region at the end of the fracture surface (D). It could be seen that samples A, B, and C were split into two separate pieces after the Charpy test, whereas sample D was not. This fact could be the sign of the high impact energy of sample D.

Table 3 — Chemical Composition of Wires, Base Metal, and Weld Metals (wt-%)

Material	C	Si	Mn	P**	S**	Mo	Cu	Al**	V**	Ti**	Nb**	Pcm

Base Metal	0.10	0.40	1.45	150	30	0.20	0.35	500	800	120	600	0.170
SG3*	0.10	0.94	1.50	40	90	0.01	0.06	—	—	60	—	—
S2Mo	0.10	0.13	1.03	120	60	0.46	0.04	—	—	20	—	—
S2Si	0.07	0.20	0.92	100	80	0.02	0.11	—	—	20	—	—
S2MoTB	0.09	0.28	1.23	100	50	0.45	0.09	—	—	1300	—	—
Weld Metal A	0.06	0.22	1.36	153	86	0.20	0.02	133	250	57	226	0.163
Weld Metal B	0.06	0.29	1.38	173	93	0.13	0.04	136	237	50	220	0.156
Weld Metal C	0.05	0.26	1.30	153	73	0.14	0.02	210	283	83	283	0.147
Weld Metal D	0.07	0.20	1.44	183	93	0.13	0.04	120	247	206	227	0.165

* The SG3 filler metal was used for tack welds by GMAW.
** The values are in ppm.

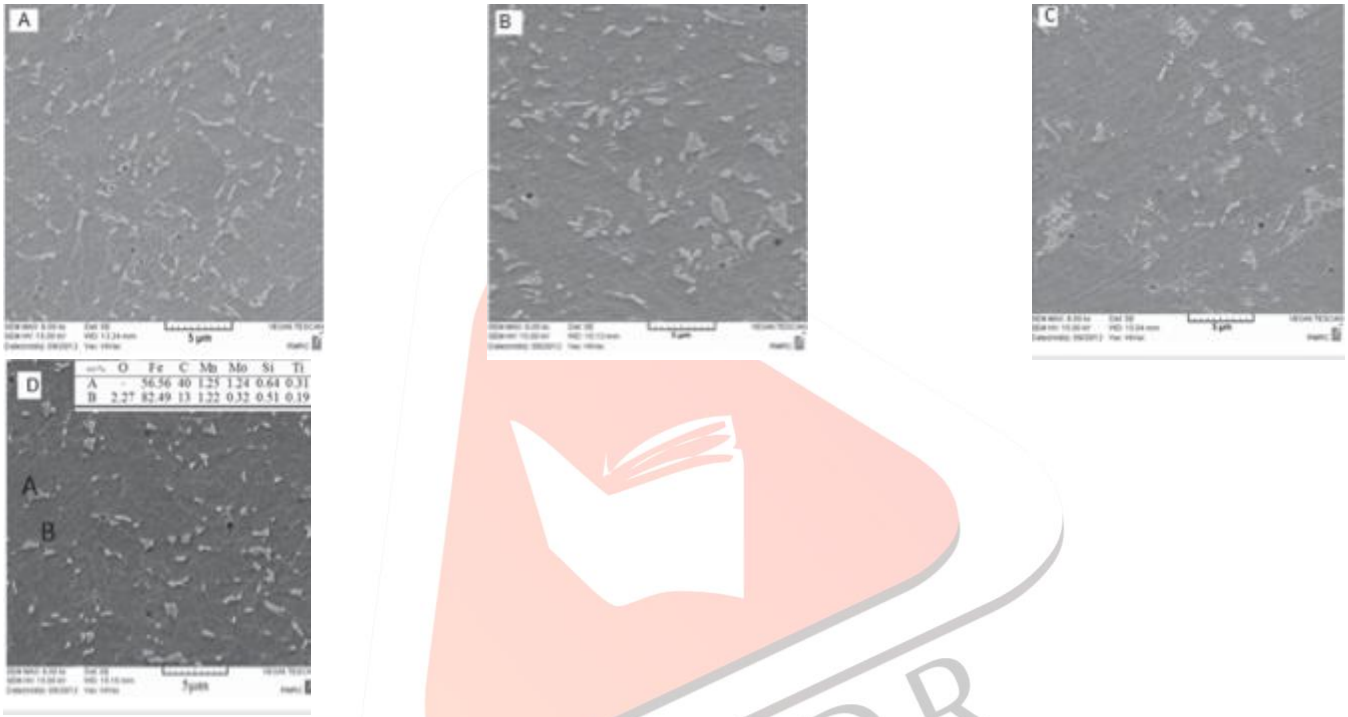

Fig 7-SEM micrographs of WM after electro-etching. The EDS result of selected points can be seen in specimen D
A-specimen A B-specimen B C-specimen C D-specimen D

Table 4 — Approximate Distribution of Different Phases in Weld Metals

Specimen	%AF	OD %F	%FSP	%AF	ID%PF	%FSP
A	61	25	14	69	21	10
B	45	38	17	54	28	18
C	48	28	24	51	29	20
D	80	12	8	84	10	6

Table 5 — Mechanical Properties of Weld Metals

Specimen	ID	OD YS(MPa)		HAZ	UTS(MPa)	%EI
A	231	215	208	563	630	28
B	231	217	213	534	609	25
C	231	214	206	534	606	28
D	245	220	209	595	649	26

DISCUSSION

According to Figs. 2 and 3, it is clear the microstructures were dominated by different morphologies of ferrite. The AF matrix is described by small effective grain size with high angle boundaries, high density of dislocations, and chaotic structure (Refs. 12, 30, 31). This unique microstructural characteristic has pre- vented crack propagation (Refs. 32, 33). Weld metals A and D presented more than 60% acicular ferrite, while specimens B and C showed large amounts of PF in their microstructures (Table 4).

The addition of titanium in specimen D promoted the formation of acicular ferrite, and this phase was the major constituent of the microstructure. Al- though molybdenum could form nucleation sites for AF (Ref. 17), by comparing specimens A and D it seems that the effect of titanium is more important.

Weld metal D was fabricated using filler metal S2Mo TB. In this filler material, boron is used to suppress the formation of grain boundary ferrite and ferrite side plates (Refs. 19, 22); also, it is liable to be oxidized and nitrified. Therefore, titanium is added to the weld to protect boron. Previous studies have shown the addition of Ti increased the nucleation of AF, and beyond the optimum range of Ti (0.02–0.05%), the recovery of Mn was increased (Ref. 8). For both actions of titanium, i.e., the protection of boron and the nucleation of acicular ferrite, there is a need for more titanium addition to a weld metal. How- ever, it has been reported that the level of Ti should be well controlled because the unsuitable addition will produce coarse TiN particles that induce cleavage fracture (Ref. 20).

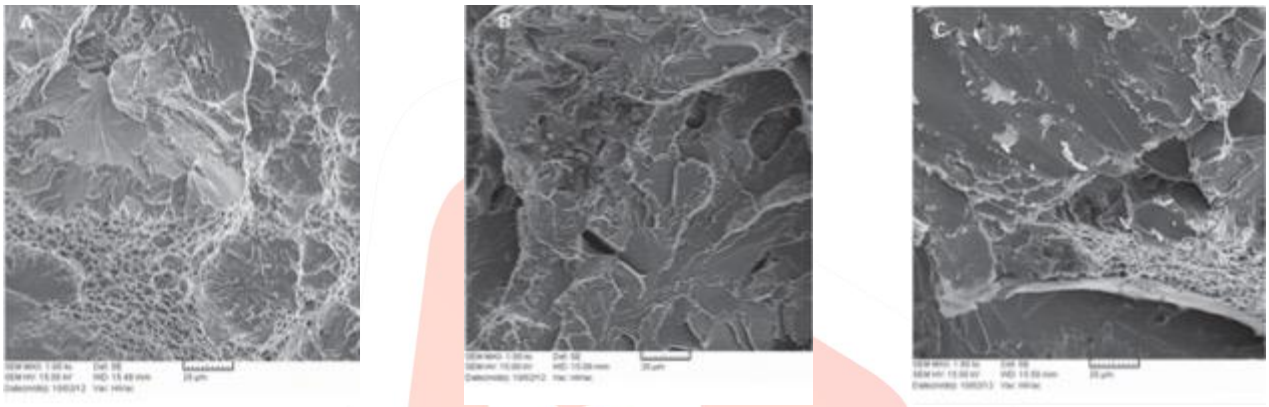

Fig 8- SEM Micrographs of Charpy impact fracture surface at -30 C

A-Specimen A B-Specimen B C-Specimen C

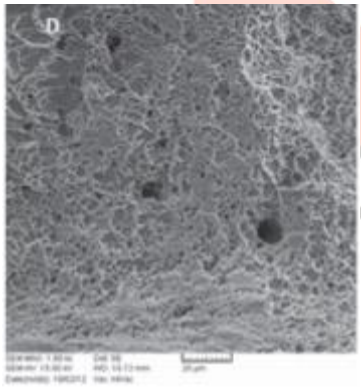

D-Specimen D

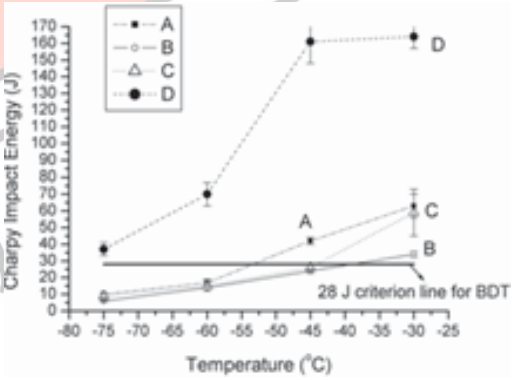

Fig 9-The impact energy vs test temperatures for welds A-D

Polygonal ferrite was typically polygonal or plate-like in shape, which was nucleated at either austenite grain boundaries or intra granular regions. It has been reported that PF phase was deleterious to toughness because of its little resistance to cleavage crack propagation (Refs. 12, 30). Ferrite with aligned second phase was formed on the grain boundaries and had a lath-like morphology. The microstructures like FSP or bainite with the parallel plates and low angle boundaries showed low impact toughness (Ref. 12). Referring to Table 3, carbon was almost constant in all specimens. The Mn contents remained in the range of 1.30–0.44% for all WMs. Manganese is one of the most common alloying elements in steels and acts as a carbide former and austenite stabilizer. Also, it has been found that silicon could slightly retard the bainite formation (Ref. 34). In this investigation, Si content of WMs reached as high as 0.29% for specimen B. According to the Ellingham diagram, the tendencies of Si and Ti to react with oxygen are nearly alike. Therefore, the competition between formation of SiO_2 and TiO_2 could reduce the number of TiO_2 particles. Titanium-based inclusions were favorable sites for the nucleation of acicular ferrite (Refs. 2, 6, 8), and this reduction in the amount of nucleation sites affected the microstructure of specimen B and C. Therefore, the amounts of PF and FSP were increased in the microstructure of welds B and C.

Different reactions could take place in the weld pool and form various inclusions in the weld metal. Some inclusions could facilitate the intra granular nucleation of AF and pin austenite grain boundaries, resulting in a reduced grain size and increased strength and tough- ness (Refs. 12, 13). It has been reported that 0.002 wt-% Ti in WM did not yield significant amount of Ti in

the inclusions (Ref. 32). The chemical composition of inclusions in each specimen were examined using EDS. The results showed that the major constituent elements were Fe, O, C, Ti, Si, Al, Mn, and Mo. Among these elements, titanium was more useful for the formation of AF. Weld metal D showed approximately 0.0206% Ti and the highest percentage of acicular ferrite in the microstructure. The nature of inclusions was complex and multiphase, and it was difficult to provide their complete characterizations through EDS analysis without more supporting analytical studies.

Figure 6 shows the SEM-EDS analysis of one inclusion with a size of 2 μm. It has been reported (Refs. 33, 35) that the appropriate size of nonmetallic Ti- containing inclusions for AF nucleation is between 0.2 and 3 μm. When the size of nonmetallic inclusion was less than 0.2 μm, the decrease in free energy barrier for the nucleation of AF and development of solute-depleted zones within the austenite grain was insufficient (Ref. 33). EDS analyses revealed these inclusions were complex oxides, which mainly consisted of Ti, Fe, Mn, Si, and O. It was also found the inclusions absorbed manganese. It seems the precipitation of MnS at titanium oxides might result in the depletion of manganese, which in turn promotes the nucleation of AF.

Figure 7 shows the SEM micrographs of WMs that are etched through electro- etching. The ferrite matrix, M/A is- lands, and carbides (if they exist) could be observed in light-black-, white-, and dark-black-colored parts, respectively. The size of M/A islands in weld metal D was the smallest among all specimens and showed the average size of about 2 μm. This value for specimens A, B, and C was approximately 3, 4, and 3 μm, respectively. The partitioning of carbon during growth of acicular ferrite could enrich the carbon content of austenite. This austenite transforms to martensite on cooling. It has been declared that the size and distribution of M/A in the matrix could affect the fracture process at low temperatures; the larger the size of M/A, the smaller the load to initiate new crack nuclei (Refs. 4, 36).

It has been reported that the microstructure of the HAZ is affected by both weld thermal cycle and chemical composition of the steel (Ref. 37). It has been observed that the addition of Ti could control the grain size of austenite in the coarse-grained HAZ and prevent the decrease in toughness (Ref. 38). In this work, different filler metal combinations did not change the microstructural characterization of the HAZ and the predominant microstructure was a combination of ferrite and M/A constituents in all specimens — Fig. 4. The Vickers hardness of any regions of the HAZ was in the range of 185–205 HV10. This indicated the HAZ was not significantly influenced by the addition of Ti. The fraction of M/A phase in the HAZ was smaller than the critical value (i.e., 6%) proposed by Zhu et al. (Ref. 38) for impairing the HAZ toughness.

According to Table 5, although the hardness range of ID was the highest, the hardness values were lower than the acceptance criterion (248 HV) for these pipelines in accordance with NACE MR0175. Therefore, the risk of cracking in sour service applications could be reduced. The highest hard- ness was related to specimen D and no hard spot was found in any specimens. The fracture surface of the Charpy im- pact samples at –30°C revealed that the fracture mode of samples A, B, and C were quasi-cleavage, cleavage, and qua- si-cleavage, respectively; while in the case of sample D, the fracture surface showed a dimpled appearance — Fig. 8. Also, decreasing the temperature ex- tended the brittle area in all fractured surfaces. Sample D was more ductile than samples A, B, and C in all applied temperatures, i.e., –30°C, –45°C, –60°C, and –75°C. The increased amount of AF in the microstructure of specimen D could be responsible for this behavior. It has been reported (Ref. 31) that high angle grain boundaries and fine packet size as well as the interweave AF microstructure showed good impact toughness and finer cleavage facet com- pared to the coarse grain boundary allotriomorphic ferrite and Widmanstätten ferrite.

The absorbed Charpy impact energies have been plotted against testing temperatures — Fig. 9. At –30˚C, the lowest and highest impact energies were 34 J (specimen B) and 164 J (specimen D). At –45˚C, the impact energy of specimens B and C was dropped from 34 and 59 J to 24 and 26 J, respectively. Since the brittle-ductile transition (BDT) temperature is calculated based on the impact energy of 28 J (Ref. 39), the horizontal line in the diagram in Fig. 9 represents this criterion. There- fore, the temperature of about –45°C could be considered as the BDT temperature of weldments B and C. By decreasing the temperature to –60°C, the impact energy of specimen A was dropped to 17 J; whereas, for specimen D, the impact energy had the remarkable value of 70 J. It was observed that the best impact properties were obtained by specimen D.

According to the mechanical proper- ties results (Table 5), the yield strength, tensile strength, hardness, and impact energy were well improved in specimen D. This behavior is related to the in- crease of AF in the microstructure as well as the grain refinement phenome- non due to the more dispersed Ti-containing inclusions. The microstructure containing acicular ferrite has a good Charpy impact toughness, which is mainly related to small effective packet size and fine interlocking pattern of AF.

The experimental results revealed that the more acicular ferrite was found in the microstructure, the higher mechanical properties were achieved. By using Ti-B wires, the amount of PF was reduced partially and replaced by AF. This fact was attributed to the increased number of AF nucleation sites (Ti-containing inclusions) and the pinning effect of B on the grain boundaries. From the pipeline fabricator point of view, the good mechanical properties of the welds compensate for the higher cost of Ti-B filler metals.

CONCLUSIONS

The effect of filler material on the microstructure and mechanical properties of weld metal was studied in the practical TSAW process. The main results of the present study could be summarized as follows:

1. Although a mixed microstructure of PF, AF, FSP, and M/A islands was obtained in each WM, acicular ferrite was the dominant microstructure. The micro structure of the HAZ in all specimens was a combination of ferrite, bainite, and martensite / austenite (M/A) constituents.
2. The major constituent elements of inclusions were Fe, O, C, Ti, Si, Al, Mn, and Mo. The increased amount of titanium promoted the formation of AF and improved the mechanical properties.
3. The formation of oxide particles with a size of 2 μm increased the nucleation of AF. Also, the microstructure refinement was encouraged.
4. The increased amount of AF promoted strength, toughness, and impact properties of the weldments. For

the microstructure with 80% acicular ferrite, the impact energy was about 70 J at –60°C.

ACKNOWLEGEMENT

The authors wish to express appreciation to Research Deputy of Ferdowsi University of Mashhad for sup- porting this project by grant No. 2/26379-31/02/92. Also, the authors are thankful to Mahshahr Pipe Mill (MPM) Company for providing the materials and laboratory facilities in its factory. Thanks are also due to A. Amini for his assistance with the experimental works.

REFERENCES

[1] Zhao, M. C., Yang, K., and Shan, Y. Y. 2003. Comparison on strength and tough- ness behaviors of micro alloyed pipeline
[2] Beidokhti, B., Kokabi, A. H., and Dolati, A. 2014. A comprehensive study on the microstructure of high strength low alloy pipeline welds. *Journal of Alloys and Com- pounds* 597: 142–147.
[3] Yu, H., Sun, Y., Chen, Q., Jiang, H., and Zhang, L. 2006. Precipitation behaviors of X70 acicular ferrite pipeline steel. *Journal of University of Science and Technology Beijing, Mineral, Metallurgy, Material* 13(6): 523–527.
[4] Shin, S. Y., Hwang, B., Kim, S., and Lee, S. 2006. Fracture toughness analysis in transition temperature region of API X70 pipeline steels. *Materials Science and Engineering A* 429: 196–204.
[5] Abedi, S. S., Abdolmaleki, A., and Adibi, N. 2007. Failure analysis of SCC and SRB induced cracking of a transmission oil products pipeline. *Engineering Failure Analysis* 14(1): 250–261.
[6] Beidokhti, B., Koukabi, A. H., and Dolati, A. 2009. Effect of titanium addition on the microstructure and inclusion forma- tion in submerged arc welded HSLA pipeline steel. *Journal of Materials Processing and Technology* 209(8): 4027–4035.
[7] Bhole, S. D., Nemade, J. B., Collins, L., and Liu, C. 2006. Effect of nickel and molybdenum additions on weld metal toughness in a submerged arc welded HSLA line-pipe steel. *Journal of Materials Processing and Technology* 173(1): 92–100.
[8] Beidokhti, B., Koukabi, A. H., and Dolati, A. 2009. Influences of titanium and manganese on high strength low alloy SAW weld metal properties. *Materials Characterization* 60(3): 225–233.
[9] Zhao, M., and Yang, K. 2005. Strengthening and improvement of sulfide stress cracking resistance in acicular ferrite pipeline steels by nano sized carbo nitrides. *Scripta Materialia* 52(9): 881–886.
[10] Contreras, A., Albiter, A., Salazar, M., and Pérez, R. 2005. Slow strain rate corrosion and fracture characteristics of X-52 and X-70 pipeline steels. *Materials Science and Engineering A* 407: 45–52.
[11] Zhong, Y., Xiao, F., Zhang, J., Shan, Y., Wang, W., and Yang, K. 2006. In situ TEM study of the effect of M/A films at grain boundaries on crack propagation in an ultra-fine acicular ferrite pipeline steel. *Acta Materialia* 54(2): 435–443.
[12] Avazkonandeh-Gharavol, M. H., Had- dad-Sabzevar, M., and Haerian, A. 2009. Effect of copper content on the microstructure and mechanical properties of multi pass MMA low alloy steel weld metal deposits. *Materials & Design* 30(6): 1902–1912
[13] Bose-Filho, W. W., Carvalho, A. L. M., and Strangwood, M. 2007. Effects of alloying elements on the microstructure and inclusion formation in HSLA multi pass welds. *Materials Characterization* 58(1): 29–39.
[14] Yu, H. 2008. Influences of micro structure and texture on crack propagation path of X70 acicular ferrite pipeline steel. *Journal of University of Science and Technology Beijing, Mineral, Metallurgy, Material* 15: 683–687
[15] Nayak, S. S., Misra, R. D. K., Hartmann, J., Siciliano, F., and Gray, J. M. 2008. Microstructure and properties of low manganese and niobium containing HIC pipeline steel. *Materials Science and Engineering A* 494: 456–463
[16] Zhao, M. C., Yang, K., and Shan, Y. 2002. The effects of thermo-mechanical control process on microstructures and mechanical properties of a commercial pipeline steel. *Materials Science and Engineering A* 335: 14–20
[17] Shanmugam, S., Misra, R. D. K., Hartmann, J., and Jansto, S. G. 2006. Microstructure of high strength niobium-containing pipeline steel. *Materials Science and Engineering A* 441: 215–229.
[18] Babu, S. S. 2004. The mechanism of acicular ferrite in weld deposits. *Current Opinion in Solid State and Materials Science* 8: 267–278.
[19] Zhang, D., Terasaki, H., and Komizo, Y. 2010. In situ observation of the formation of intra granular acicular ferrite at non-metallic inclusions in C–Mn steel. *Acta Materailia* 58: 1369–1378.
[20] Yan, W., Shan, Y. Y., and Yang, K. 2005. Effect of TiN inclusions on the impact toughness of low-carbon micro alloyed steels. *Metallurgical and Materials Transactions A* 37: 2147–2158.
[21] Lee, J. L., and Pan, Y. T. 1993. Effect of sulfur content on the microstructure and toughness of simulated heat-affected zone in Ti-killed steels. *Metallurgical Transactions A* 24: 1399–1408.
[22] Peng, Y., Chen, W., and Xu, Z. 2001. Study of high toughness ferrite wire for sub- merged arc welding of pipeline steel. *Materials Characterization* 47: 67–73.
[23] Surian, E., Rissone, M. R. D., and Vedia, L. D. 2005 Influence of molybdenum on ferritic high-strength SMAW all- weld-metal properties. *Welding Journal* 84(4): 53-s to 62-s.
[24] Evans, G. M. 1991. The effect of nick- el on microstructure and properties of C– Mn all-weld metal deposits. *Welding Research Abroad* 41: 70–83.
[25] Junhua, K., Lin, Z., Bin, G., Pinghe, L., Aihua, W., and Changsheng, X. 2004 Influence of Mo content on microstructure and mechanical properties of high strength pipeline steel. *Materials & Design* 25(8): 723–728.
[26] Snyder, J. P., and Pense, W. 1982. The effects of titanium on submerged arc weld metal. *Welding Journal* 61(7): 2s to 211-s.
[27] Shim, J. H., Cho, Y. W., Shim, J. D., Oh, Y. J., Byun, J. S., and Lee, D. N. 2001. Effects of Si and Al on acicular ferrite formation in C-Mn steel. *Metallurgical and Materials Transactions A* 32(1): 75–83.
[28] API. 2004. Specification for Line Pipe— API Specification 5L. 43rd ed., Washing- ton, DC: American Petroleum Institute.
[29] Ale, R. M., Rebello, J. M. A., and Charlier, J. 1996. A metallographic technique for detecting martensite-austenite constituents in the weld heat-affected zone of a micro-alloyed steel. *Materials Characterization* 37: 89–93.

[30] Xiao, F. R., Liao, B., Shan, Y. Y., Qiao, G. Y., Zhong, Y., Zhang, C., and Yang, K. 2006. Challenge of mechanical properties of an acicular ferrite pipeline steel. *Materials Science and Engineering A* 431: 41–52.
[31] Wan, X. L., Wang, H. H., Cheng, L., and Wu, K. M. 2012. The formation mechanisms of interlocked microstructures in low-carbon high-strength steel weld metals. *Materials Characterization* 67: 41–51.
[32] St-Laurent, S., and L'Espérance, G. 1992. Effects of chemistry, density and size distribution of inclusions on the nucleation of acicular ferrite of C-Mn steel shielded- metal-arc-welding weldments. *Materials Science and Engineering A* 149: 203–216.
[33] Fattahi, M., Nabhani, N., Hosseini, M., Arabian, N., and Rahimi, E. 2013. Effect of Ti-containing inclusions on the nucleation of acicular ferrite and mechanical properties of multi pass weld metals. *Micron* 45: 107–114.
[34] Wang, J., Van Der Wolk, P. J., and Van Der Zwaag, S. 2000. On the influence of alloying elements on the bainite reaction in low alloy steels during continuous cooling. J*ournal of Materials Science* 35(17): 4393–4404.
[35] Shim, J. H., Cho, Y. W., Chung, S. H., Shim, J. D., and Lee, D. N. 1999. Nucleation of intra granular ferrite at Ti_2O_3 particle in low carbon steel. *Acta Materialia* 47(9): 2751–2760.
[36] Chen, J. H., Kikuta, Y., Araki, T., Yoneda, M., and Matsuda, Y. 1984. Micro- fracture behaviour induced by M-A constituent (island martensite) in simulated welding heat affected zone of HT80 high strength low alloyed steel. *Acta Metallurgica* 32: 1779–1788.
[37] Mohammadi, F., Eliyan, F. F., and Al- fantazi, A. 2012. Corrosion of simulated weld HAZ of API X-80 pipeline steel. *Corrosion Science* 63: 323–333.
[38] Zhu, Z., Kuzmikova, L., Li, H., and Barbaro, F. J. 2013. The effect of chemical composition on microstructure and proper- ties of inter critically reheated coarse-grained heat-affected zone in X70 steels. *Metallurgical and Materials Transactions B* 45(1): 229–235.
[39] Panontin, T. L., and Sheppard, S. D. 1999. Fatigue and Fracture Mechanics. 29th Vol., PA, ASTM International.